

MultiMesh Finite Elements with Flexible Mesh Sizes

August Johansson^{a,*}, Mats G. Larson^b, Anders Logg^c

^a*SINTEF Digital, Mathematics and Cybernetics, PO Box 124 Blindern, 0314 Oslo, Norway*

^b*Department of Mathematics and Mathematical Statistics, Umeå University, 90187 Umeå, Sweden*

^c*Department of Mathematical Sciences, Chalmers University of Technology and University of Gothenburg, 41296 Göteborg, Sweden*

Abstract

We analyze a new framework for expressing finite element methods on arbitrarily many intersecting meshes: multimesh finite element methods. The multimesh finite element method, first presented in [30], enables the use of separate meshes to discretize parts of a computational domain that are naturally separate; such as the components of an engine, the domains of a multiphysics problem, or solid bodies interacting under the influence of forces from surrounding fluids or other physical fields. Furthermore, each of these meshes may have its own mesh parameter. In the present paper we show that the proposed formulation is stable without assumptions on the relative sizes of the mesh parameters. In particular, we prove optimal order *a priori* error estimates as well as optimal order estimates of the condition number. Throughout the analysis, we trace the dependence of the number of intersecting meshes. Numerical examples are included to illustrate the stability of the method.

Keywords: FEM, unfitted mesh, non-matching mesh, multimesh, CutFEM, Nitsche

1. Introduction

The multimesh finite element method presented in [30] extends the finite element method to arbitrarily many overlapping and intersecting meshes. This is of great value for problems that are naturally formulated on domains composed of *parts*,

*Corresponding author

Email addresses: august.johansson@sintef.no (August Johansson),
mats.larson@umu.se (Mats G. Larson), logg@chalmers.se (Anders Logg)

such as complex domains composed of simpler parts that may be more easily meshed than their composition. This is of particular importance when the parts are moving, either relative to each other or relative to a fixed background mesh, as part of a time-dependent simulation or optimization problem [18]. Figure 1 provides some illustrative examples.

The mathematical basis for the multimesh element method is Nitsche’s method [41], which is here used for weakly enforcing the interface conditions between the different meshes. Nitsche’s method is also the basis for discontinuous Galerkin methods [2] which also may be cast in a setting of non-matching meshes [3, 31, 25, 45, 46]. In addition, Nitsche’s method is also the foundation of the finite element method on cut meshes, CutFEM, see for example [26, 27, 4, 13, 12, 15] or [11, 8] for overviews. The analysis presented in this paper indeed have similarities with the techniques used for analyzing CutFEM. See also [38, 32] where related formulations for the Stokes problem are presented and analyzed.

Several methods for treating the interface problems with non-matching and multiple meshes exist in literature. There are techniques based on XFEM [39, 23, 14, 34, 22]; domain decomposition [44, 5] or [1, 29] and the references therein; the finite cell method [47, 19, 42, 48, 17, 16]; the immersed interface method [35, 36]; the classical immersed boundary methods and its variants using finite elements [43, 7, 6, 28, 37, 49]; the s-version of the finite element method [20, 21] and fictitious domain methods [24, 40, 33], to name a few.

In the remainder of this paper, we analyze the multimesh finite element method for the Poisson problem for an arbitrary number of intersecting meshes. The formulation presented here differs from the original formulation in that we here allow for the meshes to have arbitrarily different mesh sizes. This is illustrated in the numerical examples. We will start with reviewing the notation from [30] in section 2, following a presentation of the multimesh finite element method 3. We then proceed to establish standard results such as consistency and continuity of the method in section 4. Showing coercivity, interpolation error estimates, *a priori* error estimates and a condition number estimate require more work, which is why we dedicate individual sections to these in 5, 6, 7, and 8 correspondingly. We end the paper with numerical results in section 9, conclusions in section 10 and acknowledgements in section 11.

2. Notation

We first review the notation for domains, interfaces, meshes, overlaps, function spaces and norms used to formulate and analyze the multimesh finite element method. For a more detailed exposition, we refer to [30].

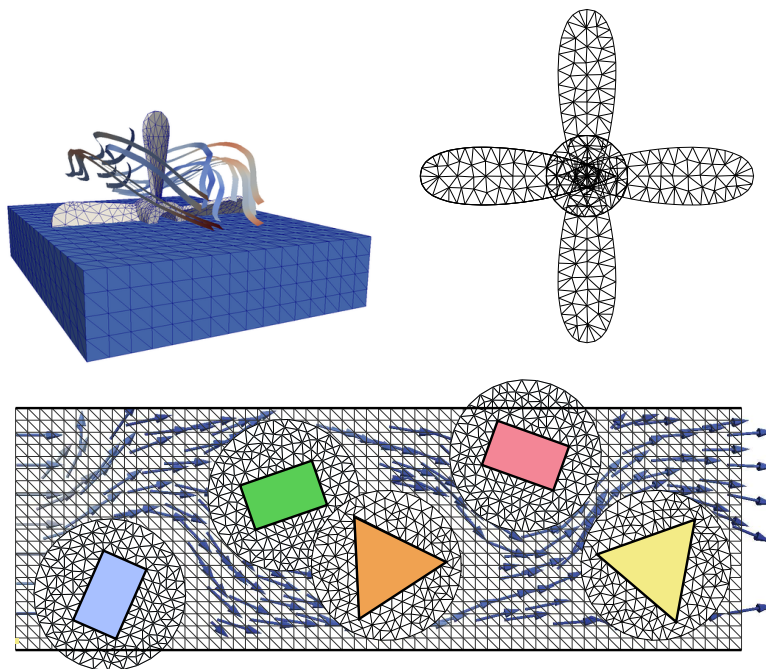


Figure 1: (Top left) The flow around a propeller may be computed by immersing a mesh of the propeller into a fixed background mesh. (Top right) The geometry of a composite object may be discretized by superimposing meshes of each component. (Bottom) The interaction of a set of solid bodies may be simulated using individual meshes that move and intersect freely relative to each other and a fixed background mesh.

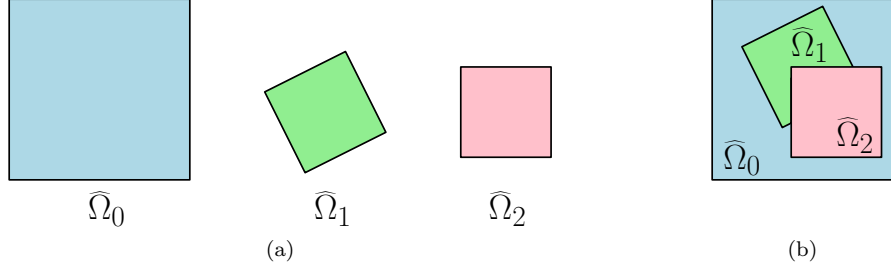


Figure 2: (a) Three polygonal predomains. (b) The predomains are placed on top of each other in an ordering such that $\widehat{\Omega}_0$ is placed lowest, $\widehat{\Omega}_1$ is in the middle and $\widehat{\Omega}_2$ is on top.

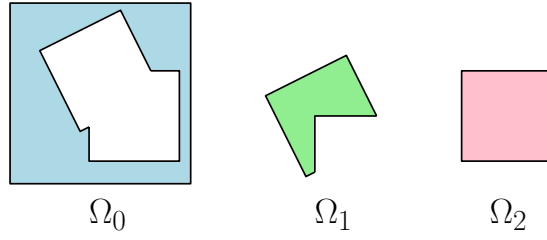


Figure 3: Partition of $\Omega = \Omega_0 \cup \Omega_1 \cup \Omega_2$. Note that $\Omega_2 = \widehat{\Omega}_2$.

Notation for domains

Let $\Omega = \widehat{\Omega}_0 \subset \mathbb{R}^d$, $d = 2, 3$, be a domain with polygonal boundary (the background domain).

Let $\widehat{\Omega}_i \subset \widehat{\Omega}_0$, $i = 1, \dots, N$ be the so-called *predomains* with polygonal boundaries (see Figure 2).

Let $\Omega_i = \widehat{\Omega}_i \setminus \bigcup_{j=i+1}^N \widehat{\Omega}_j$, $i = 0, \dots, N$ be a partition of Ω (see Figure 3).

Remark 2.1. To simplify the presentation, the domains $\Omega_1, \dots, \Omega_N$ are not allowed to intersect the boundary of Ω .

Notation for interfaces

Let the *interface* Γ_i be defined by $\Gamma_i = \partial\widehat{\Omega}_i \setminus \bigcup_{j=i+1}^N \widehat{\Omega}_j$, $i = 1, \dots, N-1$ (see Figure 4a).

Let $\Gamma_{ij} = \Gamma_i \cap \Omega_j$, $i > j$ be a partition of Γ_i (see Figure 4b).

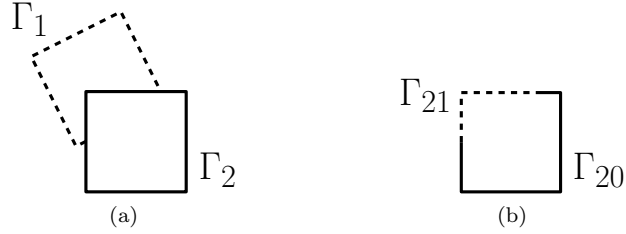


Figure 4: (a) The two interfaces of the domains in Figure 2: $\Gamma_1 = \partial\widehat{\Omega}_1 \setminus \widehat{\Omega}_2$ (dashed line) and $\Gamma_2 = \partial\widehat{\Omega}_2$ (filled line). Note that Γ_1 is not a closed curve. (b) Partition of $\Gamma_2 = \Gamma_{20} \cup \Gamma_{21}$.

Notation for meshes

Let $\widehat{\mathcal{K}}_{h,i}$ be a quasi-uniform [9] *premesh* on $\widehat{\Omega}_i$ with mesh parameter $h_i = \max_{K \in \widehat{\mathcal{K}}_{h,i}} \text{diam}(K)$, $i = 0, \dots, N$ (see Figure 5a). Let $h = \max_{0 \leq i \leq N} h_i$. Let $\mathcal{K}_{h,i} = \{K \in \widehat{\mathcal{K}}_{h,i} : K \cap \Omega_i \neq \emptyset\}$, $i = 0, \dots, N$ be the *active meshes* (see Figure 5b). The *multimesh* is formed by the active meshes placed in the given ordering (see Figure 6b). Let $\Omega_{h,i} = \bigcup_{K \in \mathcal{K}_{h,i}} K$, $i = 0, \dots, N$ be the *active domains*.

Notation for overlaps

Let \mathcal{O}_i denote the *overlap* defined by $\mathcal{O}_i = \Omega_{h,i} \setminus \Omega_i$, $i = 0, \dots, N - 1$. Let $\mathcal{O}_{ij} = \mathcal{O}_i \cap \Omega_j = \Omega_{h,i} \cap \Omega_j$, $i < j$ be a partition of \mathcal{O}_i . For $i < j$, let

$$\delta_{ij} = \begin{cases} 1, & \mathcal{O}_{ij} \neq \emptyset, \\ 0, & \text{otherwise,} \end{cases} \quad (2.1)$$

be a function indicating which overlaps are non-empty. For ease of notation, we further let $\delta_{ii} = 1$ for $i = 0, \dots, N$.

Let $N_{\mathcal{O}} = \max(\max_i \sum_j \delta_{ij}, \max_j \sum_i \delta_{ij})$ be the maximum number of overlaps. Note that $N_{\mathcal{O}}$ is bounded by N but is smaller if not all meshes intersect with each other.

Let $N_{\mathcal{O}_i} = \sum_{j=0}^{i-1} \delta_{ji}$, i.e., the number of meshes below mesh i with non-empty intersection.

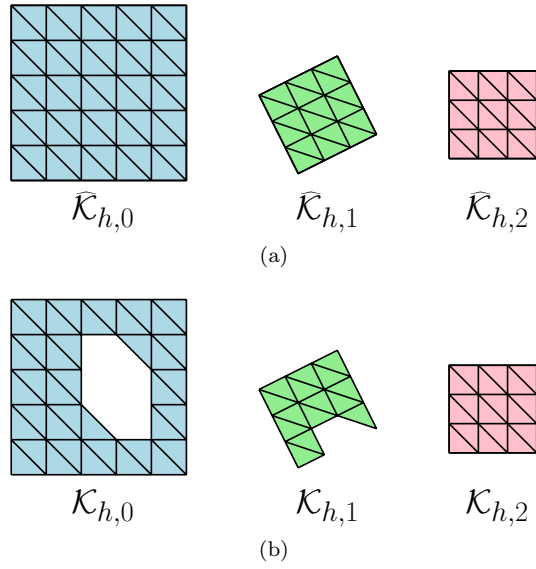


Figure 5: (a) The three premeshes. (b) The corresponding active meshes (cf. Figures 2 and 3).

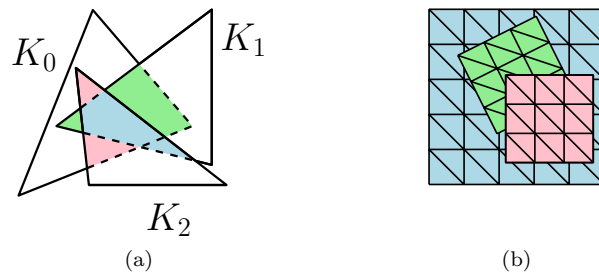


Figure 6: (a) Given three ordered triangles K_0 , K_1 and K_2 , the overlaps are \mathcal{O}_{01} in green, \mathcal{O}_{02} in red and \mathcal{O}_{12} in blue. (b) The multimesh of the domains in Figure 2b consists of the active meshes in Figure 5b.

Notation for function spaces

Let $V_{h,i}$ be a continuous piecewise polynomial finite element space on $\mathcal{K}_{h,i}$.

Let the multimesh finite element space V_h be defined by $V_h = \bigoplus_{i=0}^N V_{h,i}$.
An element $v \in V_h$ is a tuple (v_0, \dots, v_N) .

The inclusion $V_h \hookrightarrow L^2(\Omega)$ is defined by $v(x) = v_i(x)$ for $x \in \Omega_i$.

Notation for jumps and averages

The jump and average operators on V_h are defined by

$$[v] = v_i - v_j \quad i < j, \quad (2.2)$$

$$\langle n_i \cdot \nabla v \rangle = (\kappa_i n_i \cdot \nabla v_i + \kappa_j n_i \cdot \nabla v_j), \quad (2.3)$$

where v_i and v_j are the finite element solutions on represented on the active meshes $\mathcal{K}_{h,i}$ and $\mathcal{K}_{h,j}$. The weights κ_i and κ_j are defined by

$$\kappa_l = \frac{h_l}{h_i + h_j} \quad l = i, j, \quad (2.4)$$

and we note that

$$\kappa_i + \kappa_j = 1. \quad (2.5)$$

Notation for norms

Let $c > 0$ and $C > 0$ be constants. The inequality $x \leq Cy$ is denoted by $x \lesssim y$. The equivalence $cx \leq y \leq Cx$ is denoted by $x \sim y$.

Let $W_p^s(X)$ denote the standard Sobolev spaces on X with norm denoted by $\|\cdot\|_{W_p^s(X)}$ and semi-norm $|\cdot|_{W_p^s(X)}$. The special case $p = 2$ is denoted by $H^s(X)$ and the space with $p = 2$ and zero trace is denoted by $H_0^s(X)$ (see also e.g. [9, 10]). The Euclidean norm on \mathbb{R}^N is denoted by $|\cdot|_N$. The corresponding inner products are labeled accordingly. The same notation is used for the Lebesgue measure and absolute value. It will be clear from the argument which is used.

We shall make use of the following custom norms. We first let $\|\cdot\|_{s_h}$ denote the semi-norm defined by

$$\|v\|_{s_h}^2 = \sum_{i=0}^{N-1} \sum_{j=i+1}^N \|[\nabla v]\|_{\mathcal{O}_{ij}}^2, \quad (2.6)$$

and we let $\|\cdot\|_h$ denote the norm

$$\|v\|_h^2 = \sum_{i=0}^N \|v_i\|_{\Omega_{h,i}}^2. \quad (2.7)$$

Note the relation $s_h(v, v) = \beta_1 \|v\|_{s_h}^2$ between the stabilization term s_h and the norm $\|\cdot\|_{s_h}$ (see Section 3). Also note that for the norm $\|\cdot\|_h$, the domain of integration extends to each active domain $\Omega_{h,i}$, meaning that each overlap will be counted (at least) twice.

The definition of the energy norm will be defined after the presentation of the finite element method.

3. Finite element method

As a model problem we consider the Poisson problem

$$-\Delta u = f \quad \text{in } \Omega, \quad (3.1a)$$

$$u = 0 \quad \text{on } \partial\Omega, \quad (3.1b)$$

where $\Omega \subset \mathbb{R}^d$ is a polygonal domain. The multimesh finite element method for (3.1) is to find $u_h \in V_h$ such that

$$A_h(u_h, v) = l_h(v) \quad \forall v \in V_h, \quad (3.2)$$

where

$$A_h(v, w) = a_h(v, w) + s_h(v, w), \quad (3.3)$$

$$a_h(v, w) = \sum_{i=0}^N (\nabla v_i, \nabla w_i)_{\Omega_i} \quad (3.4)$$

$$\begin{aligned} & - \sum_{i=1}^N \sum_{j=0}^{i-1} (\langle n_i \cdot \nabla v \rangle, [w])_{\Gamma_{ij}} + ([v], \langle n_i \cdot \nabla w \rangle)_{\Gamma_{ij}} \\ & + \sum_{i=1}^N \sum_{j=0}^{i-1} \beta_0 (h_i + h_j)^{-1} ([v], [w])_{\Gamma_{ij}}, \end{aligned}$$

$$s_h(v, w) = \sum_{i=0}^{N-1} \sum_{j=i+1}^N \beta_1 ([\nabla v], [\nabla w])_{\mathcal{O}_{ij}}, \quad (3.5)$$

$$l_h(v) = \sum_{i=0}^N (f, v_i)_{\Omega_i}. \quad (3.6)$$

Here, $\beta_0 > 0$ is the Nitsche (interior) penalty parameter and $\beta_1 > 0$ is a stabilization parameter.

4. Energy norm, consistency, Galerkin orthogonality and continuity

Let $\|\cdot\|_h$ denote the energy norm defined by

$$\begin{aligned} \|v\|_h^2 = & \underbrace{\sum_{i=0}^N \|\nabla v_i\|_{\Omega_i}^2}_I + \underbrace{\|v\|_{s_h}^2}_{II} \\ & + \underbrace{\sum_{i=1}^N \sum_{j=0}^{i-1} (h_i \|\nabla v_i\|_{\Gamma_{ij}}^2 + h_j \|\nabla v_j\|_{\Gamma_{ij}}^2)}_{III} + \underbrace{\sum_{i=1}^N \sum_{j=0}^{i-1} (h_i + h_j)^{-1} \|[v]\|_{\Gamma_{ij}}^2}_{IV}. \end{aligned} \quad (4.1)$$

The numbering of the terms will be used to alleviate the analysis of the proposed method.

We may easily establish the consistency, Galerkin orthogonality and continuity of the form A_h .

Proposition 4.1 (Consistency). *The form A_h is consistent; that is,*

$$A_h(u, v) = l_h(v) \quad \forall v \in V_h, \quad (4.2)$$

where $u \in H_0^1(\Omega)$ is the weak solution of (3.1).

Proof. The result follows from (2.5), integration by parts and noting that the jump terms vanish for the exact solution u . \square

Proposition 4.2 (Galerkin orthogonality). *The form A_h satisfies the Galerkin orthogonality; that is,*

$$A_h(u - u_h, v) = 0 \quad \forall v \in V_h, \quad (4.3)$$

where $u \in H_0^1(\Omega)$ is the weak solution of (3.1) and $u_h \in V_h$ is a solution of (3.2).

Proof. The result follows directly from Proposition 4.1 and (3.2). \square

Proposition 4.3 (Continuity). *The form A_h is continuous; that is,*

$$A_h(v, w) \lesssim \|v\|_h \|w\|_h \quad \forall v, w \in V, \quad (4.4)$$

where $V = H^{3/2+\epsilon}(\Omega) \cap V_h$.

Proof. The result follows by repeated use of the Cauchy–Schwarz inequality. \square

Remark 4.4. *Note that we have continuity not only for the functions in V_h but also for functions in $H^{3/2+\epsilon}(\Omega)$ with $\epsilon > 0$. This is due to the need of a trace inequality on $\nabla v \in H^{1/2+\epsilon}$ in the a priori estimates in Section 7. Such inequality does not hold for $\epsilon = 0$.*

5. Coercivity

To prove that the form A_h is coercive, we will make use of the following lemma.

Lemma 5.1. *For all $v \in V_h$, we have*

$$\|\nabla v\|_h^2 \lesssim N_{\mathcal{O}} \sum_{i=0}^N \|\nabla v_i\|_{\Omega_i}^2 + \|v\|_{s_h}^2. \quad (5.1)$$

Proof. Take an element $K \in \mathcal{K}_{h,i}$ and observe that $K = \cup_{j=i}^N K \cap \Omega_j$. It follows that

$$\|\nabla v_i\|_K^2 = \|\nabla v_i\|_{K \cap \Omega_i}^2 + \sum_{j=i+1}^N \|\nabla v_i\|_{K \cap \Omega_j}^2 \quad (5.2)$$

$$\leq \|\nabla v_i\|_{K \cap \Omega_i}^2 + 2 \sum_{j=i+1}^N (\|\nabla(v_i - v_j)\|_{K \cap \Omega_j}^2 + \|\nabla v_j\|_{K \cap \Omega_j}^2) \quad (5.3)$$

$$\leq 2 \sum_{j=i}^N \|\nabla v_j\|_{K \cap \Omega_j}^2 + 2 \sum_{j=i+1}^N \|\nabla(v_i - v_j)\|_{K \cap \Omega_j}^2. \quad (5.4)$$

Here we have made use of the inequality $a^2 \leq 2(a-b)^2 + 2b^2$, which follows by Young's inequality $2ab \leq a^2 + b^2$ applied to $a^2 = (a-b+b)^2 = (a-b)^2 + b^2 + 2(a-b)b$.

Summing over all elements $K \in \mathcal{K}_{h,i}$ we have

$$\|\nabla v_i\|_{\Omega_{h,i}}^2 \leq 2 \sum_{j=i}^N \|\nabla v_j\|_{\Omega_{h,i} \cap \Omega_j}^2 + 2 \sum_{j=i+1}^N \|\nabla(v_i - v_j)\|_{\Omega_{h,i} \cap \Omega_j}^2 \quad (5.5)$$

$$= 2 \sum_{j=i}^N \delta_{ij} \|\nabla v_j\|_{\Omega_{h,i} \cap \Omega_j}^2 + 2 \sum_{j=i+1}^N \|\nabla(v_i - v_j)\|_{\mathcal{O}_{ij}}^2 \quad (5.6)$$

$$\leq 2 \sum_{j=i}^N \delta_{ij} \|\nabla v_j\|_{\Omega_j}^2 + 2 \sum_{j=i+1}^N \|\nabla(v_i - v_j)\|_{\mathcal{O}_{ij}}^2, \quad (5.7)$$

where we have used $\Omega_{h,i} \cap \Omega_j = \mathcal{O}_{ij} \subseteq \Omega_j$ for $i < j$. Note that the second sum is empty for $i = N$.

Summing over all domains, we obtain by (2.1)

$$\|\nabla v\|_h^2 \leq 2 \sum_{i=0}^N \sum_{j=i}^N \delta_{ij} \|\nabla v_j\|_{\Omega_j}^2 + 2 \sum_{i=0}^{N-1} \sum_{j=i+1}^N \|\nabla(v_i - v_j)\|_{\mathcal{O}_{ij}}^2 \quad (5.8)$$

$$\leq 2N_{\mathcal{O}} \sum_{j=0}^N \|\nabla v_j\|_{\Omega_j}^2 + 2\|v\|_{s_h}^2, \quad (5.9)$$

which proves the estimate. \square

Remark 5.2. *There is a dependence on the maximum number of overlaps $N_{\mathcal{O}}$ in Lemma 5.1. In practice, $N_{\mathcal{O}}$ is of moderate size and this dependence is not an issue. The interpolation error estimates and condition number estimates (shown below) have a different kind of dependence.*

Remark 5.3. *Using an inverse bound of the form (see e.g. [9])*

$$\|v\|_{H^l(K)} \lesssim h^{m-l} |v|_{H^m(K)} \quad m, l \in \mathbb{Z}^+, \quad m \leq l, \quad (5.10)$$

one can show that the stabilization term $s_h(v, w)$ may alternatively be formulated as

$$s_h(v, w) = \sum_{i=0}^{N-1} \sum_{j=i+1}^N \beta_1 (h_i + h_j)^{-2} ([v], [w])_{\mathcal{O}_{ij}}. \quad (5.11)$$

Using Lemma 5.1, we may now proceed to prove the coercivity of the bilinear form.

Proposition 5.4 (Coercivity). *The form A_h is coercive. More precisely, for β_0 and β_1 large enough, we have*

$$\|v\|_h^2 \lesssim A_h(v, v) \quad \forall v \in V_h. \quad (5.12)$$

Proof. We first note that

$$\begin{aligned} A_h(v, v) &\geq \sum_{i=0}^N \|\nabla v_i\|_{\Omega_i}^2 + \sum_{i=1}^N \sum_{j=0}^{i-1} \beta_0 (h_i + h_j)^{-1} \| [v] \|_{\Gamma_{ij}}^2 + \beta_1 s_h(v, v) \\ &\quad - \underbrace{\sum_{i=1}^N \sum_{j=0}^{i-1} 2 |(\langle n_i \cdot \nabla v \rangle, [v])_{\Gamma_{ij}}|}_{\star}. \end{aligned} \quad (5.13)$$

Now, for $l = i$ or $l = j$, let

$$\mathcal{K}_{h,l}(\Gamma_{ij}) = \{K \in \mathcal{K}_{h,l} : K \cap \Gamma_{ij} \neq \emptyset\} \quad (5.14)$$

denote the set of elements in $\mathcal{K}_{h,l}$ which intersect Γ_{ij} . Using an inverse estimate (see [27]), we have

$$h_l \|\nabla v_l\|_{K \cap \Gamma_{ij}}^2 \lesssim \|\nabla v_l\|_K^2, \quad (5.15)$$

where the constant is independent of the position of Γ_{ij} . It follows that

$$\sum_{j=0}^{i-1} h_l \|\nabla v_l\|_{\Gamma_{ij}}^2 = \sum_{j=0}^{i-1} \delta_{ji} h_l \|\nabla v_l\|_{\Gamma_{ij}}^2 \lesssim \sum_{j=0}^{i-1} \delta_{ji} \|\nabla v_l\|_{\mathcal{K}_{h,l}(\Gamma_{ij})}^2 \leq \sum_{j=0}^{i-1} \delta_{ji} \|\nabla v_l\|_{\Omega_{h,l}}^2, \quad (5.16)$$

where we have noted that Γ_{ij} (the part of Γ_i bordering to Ω_j for $j < i$) is empty if the overlap \mathcal{O}_{ji} (the part of $\Omega_{h,j}$ intersected by Γ_i for $j < i$) is empty, as indicated by δ_{ji} .

For $l = i$, we thus obtain the estimate

$$\sum_{i=1}^N \sum_{j=0}^{i-1} h_i \|\nabla v_i\|_{\Gamma_{ij}}^2 \lesssim \sum_{i=1}^N \sum_{j=0}^{i-1} \delta_{ji} \|\nabla v_i\|_{\Omega_{h,i}}^2 \quad (5.17)$$

$$\leq \sum_{i=1}^N \left(\sum_{j=0}^N \delta_{ji} \right) \|\nabla v_i\|_{\Omega_{h,i}}^2 \quad (5.18)$$

$$= \sum_{i=1}^N N_{\mathcal{O}_i} \|\nabla v_i\|_{\Omega_{h,i}}^2 \quad (5.19)$$

$$\leq N_{\mathcal{O}} \sum_{i=0}^N \|\nabla v_i\|_{\Omega_{h,i}}^2 \quad (5.20)$$

$$= N_{\mathcal{O}} \|\nabla v\|_h^2, \quad (5.21)$$

while for $l = j$, we obtain the similar estimate

$$\sum_{i=1}^N \sum_{j=0}^{i-1} h_j \|\nabla v_j\|_{\Gamma_{ij}}^2 \lesssim \sum_{i=1}^N \sum_{j=0}^{i-1} \delta_{ji} \|\nabla v_j\|_{\Omega_{h,j}}^2 \quad (5.22)$$

$$\leq \sum_{j=0}^N \left(\sum_{i=0}^N \delta_{ji} \right) \|\nabla v_j\|_{\Omega_{h,j}}^2 \quad (5.23)$$

$$= N_{\mathcal{O}} \sum_{j=0}^N \|\nabla v_j\|_{\Omega_{h,j}}^2 \quad (5.24)$$

$$= N_{\mathcal{O}} \|\nabla v\|_h^2. \quad (5.25)$$

Proceeding with \star using the Cauchy–Schwarz inequality with weight $\epsilon(h_i + h_j)$

and Young's inequality $2ab \leq a^2 + b^2$ we obtain

$$\begin{aligned} \star &= \sum_{i=1}^N \sum_{j=0}^{i-1} 2|(\langle n_i \cdot \nabla v \rangle, [v])_{\Gamma_{ij}}| \\ &\leq \sum_{i=1}^N \sum_{j=0}^{i-1} 2\epsilon^{1/2}(h_i + h_j)^{1/2} \|\langle n_i \cdot \nabla v \rangle\|_{\Gamma_{ij}} \epsilon^{-1/2}(h_i + h_j)^{-1/2} \|[v]\|_{\Gamma_{ij}} \end{aligned} \quad (5.26)$$

$$\leq \sum_{i=1}^N \sum_{j=0}^{i-1} \epsilon(h_i + h_j) \|\langle n_i \cdot \nabla v \rangle\|_{\Gamma_{ij}}^2 + \sum_{i=1}^N \sum_{j=0}^{i-1} \epsilon^{-1}(h_i + h_j)^{-1} \|[v]\|_{\Gamma_{ij}}^2 \quad (5.27)$$

$$\lesssim \sum_{i=1}^N \sum_{j=0}^{i-1} \epsilon(h_i \|\nabla v_i\|_{\Gamma_{ij}}^2 + h_j \|\nabla v_j\|_{\Gamma_{ij}}^2) + \sum_{i=1}^N \sum_{j=0}^{i-1} \epsilon^{-1}(h_i + h_j)^{-1} \|[v]\|_{\Gamma_{ij}}^2 \quad (5.28)$$

$$\lesssim \epsilon N_{\mathcal{O}} \|\nabla v\|_h^2 + \sum_{i=1}^N \sum_{j=0}^{i-1} \epsilon^{-1}(h_i + h_j)^{-1} \|[v]\|_{\Gamma_{ij}}^2. \quad (5.29)$$

In (5.28) we used that

$$(h_i + h_j) \|\langle n_i \cdot \nabla v \rangle\|_{\Gamma_{ij}}^2 \leq 2(h_i + h_j) \kappa_i^2 \|\nabla v_i\|_{\Gamma_{ij}}^2 + 2(h_i + h_j) \kappa_j^2 \|\nabla v_j\|_{\Gamma_{ij}}^2 \quad (5.30)$$

$$\leq 2h_i \|\nabla v_i\|_{\Gamma_{ij}}^2 + 2h_j \|\nabla v_j\|_{\Gamma_{ij}}^2. \quad (5.31)$$

where we used the definition (2.4) of the weights κ_l to obtain

$$(h_i + h_j) \kappa_l^2 = \frac{h_l^2}{h_i + h_j} = \frac{h_l}{h_i + h_j} h_l \leq h_l \quad l = i, j. \quad (5.32)$$

In (5.29) we made use of (5.21) and (5.25).

By Lemma 5.1, we may now estimate the $\|\cdot\|_h$ norm in terms of the $\|\cdot\|_{\Omega}$ norm and the $\|\cdot\|_{s_h}$ norm to obtain

$$\star \lesssim \epsilon N_{\mathcal{O}}^2 \sum_{i=0}^N \|\nabla v_i\|_{\Omega_i}^2 + \epsilon N_{\mathcal{O}} \|v\|_{s_h}^2 + \epsilon^{-1} \sum_{i=1}^N \sum_{j=0}^{i-1} (h_i + h_j)^{-1} \|[v]\|_{\Gamma_{ij}}^2. \quad (5.33)$$

Combining (5.13) and (5.33), we find that

$$\begin{aligned} A_h(v, v) &\geq \sum_{i=0}^N (1 - \epsilon C N_{\mathcal{O}}^2) \|\nabla v_i\|_{\Omega_i}^2 + (\beta_1 - \epsilon C N_{\mathcal{O}}) \|v\|_{s_h}^2 \\ &\quad + \sum_{i=1}^N \sum_{j=0}^{i-1} (\beta_0 - \epsilon^{-1} C) (h_i + h_j)^{-1} \|[v]\|_{\Gamma_{ij}}^2, \end{aligned} \quad (5.34)$$

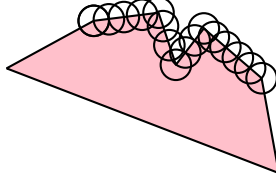


Figure 7: Balls $B_\delta(x)$ centered at $x \in \Gamma$.

and thus, by choosing ϵ small enough and then β_0 and β_1 large enough,

$$A_h(v, v) \gtrsim \sum_{i=0}^N \|\nabla v_i\|_{\Omega_i}^2 + \|v\|_{s_h}^2 + \sum_{i=1}^N \sum_{j=0}^{i-1} (h_i + h_j)^{-1} \|[v]\|_{\Gamma_{ij}}^2. \quad (5.35)$$

The coercivity now follows by noting that term *III* in (4.1) may be controlled by terms *I* and *II* as above in the estimate of \star . \square

Remark 5.5. *By continuity (4.4), coercivity (5.12) and a continuous $l_h(v)$, there exists a unique solution to (3.2) by the Lax–Milgram theorem (see e.g. [9]).*

Remark 5.6. *In view of (5.34) we note that for large β_0 we may take $\epsilon \sim \beta_0^{-1}$ and thus we can choose $\beta_1 \sim \epsilon \sim \beta_0^{-1}$.*

6. Interpolation error estimate

To construct an interpolation operator into V_h , we pick a standard interpolation operator into $V_{h,i}$,

$$\pi_{h,i} : L^2(\Omega_{h,i}) \longrightarrow V_{h,i}, \quad i = 0, 1, \dots, N, \quad (6.1)$$

where $\pi_{h,i}$ satisfies the standard interpolation error estimate (see e.g. [9])

$$\|v - \pi_{h,i}v\|_{H^m(K)} \lesssim h^{k+1-m} |v|_{H^{k+1}(\mathcal{N}_h(K))}. \quad (6.2)$$

Here, $\mathcal{N}_h(K)$ denotes the set of elements that share a vertex with K . We may then define the interpolation operator into V_h by

$$\pi_h : L^2(\Omega) \ni v \longmapsto \bigoplus_{i=0}^N \pi_{h,i}(v|_{\Omega_{h,i}}) \in V_h. \quad (6.3)$$

To prove an interpolation error estimate for π_h , we let $U_\delta(\Gamma_{ij})$ denote the tubular neighborhood of Γ_{ij} defined by

$$U_\delta(\Gamma_{ij}) = \bigcup_{x \in \Gamma_{ij}} B_\delta(x), \quad (6.4)$$

where $B_\delta(x)$ is the ball of radius δ centered at x ; see Figure 7. In addition, let

$$U_\delta(\Gamma) = \bigcup_{i,j} U_\delta(\Gamma_{ij}). \quad (6.5)$$

Proposition 6.1 (Interpolation error estimate). *The interpolation operator π_h satisfies the interpolation error estimate*

$$\|v - \pi_h v\|_h^2 \lesssim C_{h,N} \sum_{i=0}^N h_i^{2k} |v_i|_{H^{k+1}(\Omega_{h,i}) \cap W_\infty^{k+1}(U_h(\Gamma_i))}^2, \quad (6.6)$$

where

$$C_{h,N} = 1 + \max_{0 \leq i \leq N} h_i^d N_{\mathcal{O}_i} + \max_{0 \leq i \leq N} h_i |\Gamma_i|, \quad (6.7)$$

and the norm is defined by

$$|v|_{H^{k+1}(\Omega) \cap W_\infty^{k+1}(U_h(\Gamma))}^2 = |v|_{H^{k+1}(\Omega)}^2 + |v|_{W_\infty^{k+1}(U_h(\Gamma))}^2. \quad (6.8)$$

Proof. We first let $\eta = v - \pi_h v$ denote the interpolation error and recall the numbering of the terms in the definition of the energy norm $\|\cdot\|_h$ (4.1). Starting with term I , we have

$$I(\eta) = \sum_{i=0}^N \|\nabla \eta_i\|_{\Omega_i}^2 \leq \sum_{i=0}^N \|\nabla \eta_i\|_{\Omega_{h,i}}^2. \quad (6.9)$$

For term II , we have, since $\cup_{j=i+1}^N \mathcal{O}_{ij} \subseteq \Omega_{h,i}$ and $\mathcal{O}_{ij} \subseteq U_\delta(\Gamma_{ji}) \cap \Omega_j$ with $\delta \sim h_i$,

$$II(\eta) \lesssim \sum_{i=0}^{N-1} \sum_{j=i+1}^N (\|\nabla \eta_i\|_{\mathcal{O}_{ij}}^2 + \|\nabla \eta_j\|_{\mathcal{O}_{ij}}^2) \quad (6.10)$$

$$\leq \sum_{i=0}^{N-1} \|\nabla \eta_i\|_{\Omega_{h,i}}^2 + \sum_{i=0}^{N-1} \sum_{j=i+1}^N \delta_{ij} \|\nabla \eta_j\|_{U_\delta(\Gamma_{ji}) \cap \Omega_j}^2. \quad (6.11)$$

For term III , recall the inverse estimate (5.16) and note that $\mathcal{K}_{h,j}(\Gamma_{ij}) \subseteq U_\delta(\Gamma_{ij})$ with $\delta \sim h_j$. Thus,

$$III(\eta) = \sum_{i=1}^N \sum_{j=0}^{i-1} (h_i \|\nabla \eta_i\|_{\Gamma_{ij}}^2 + h_j \|\nabla \eta_j\|_{\Gamma_{ij}}^2) \quad (6.12)$$

$$\lesssim N_{\mathcal{O}} \sum_{i=1}^N \|\nabla \eta_i\|_{\Omega_{h,i}}^2 + \sum_{i=1}^N \sum_{j=0}^{i-1} \delta_{ji} \|\nabla \eta_j\|_{U_\delta(\Gamma_{ij})}^2. \quad (6.13)$$

For term IV , we first handle the jump term as in II and then proceed as for III ,

$$IV(\eta) \leq \sum_{i=1}^N \sum_{j=0}^{i-1} (h_i + h_j)^{-1} (\|\eta_i\|_{\Gamma_{ij}}^2 + \|\eta_j\|_{\Gamma_{ij}}^2) \quad (6.14)$$

$$\lesssim N_{\mathcal{O}} \sum_{i=1}^N h_i^{-2} \|\eta_i\|_{\Omega_{h,i}}^2 + \sum_{i=1}^N \sum_{j=0}^{i-1} \delta_{ji} h_j^{-2} \|\eta_j\|_{U_\delta(\Gamma_{ij})}^2. \quad (6.15)$$

Now, note that since $\Omega_{h,i} \subseteq \Omega_i \cup_{j=i+1}^N U_\delta(\Gamma_{ij})$, we have

$$\sum_{i=0}^N \|v_i\|_{\Omega_{h,i}}^2 \lesssim \sum_{i=0}^N \|v_i\|_{\Omega_i}^2 + \sum_{i=1}^N \sum_{j=0}^{i-1} \delta_{ij} \|v_i\|_{U_\delta(\Gamma_{ij})}^2. \quad (6.16)$$

Therefore, there are only two terms in $I - IV$ that need to be estimated. First

$$h_i^{2(m-1)} |\eta_i|_{H^m(\Omega_i)}^2 \lesssim h_i^{2k} |v_i|_{H^{k+1}(\Omega_i)}^2 \quad m = 0, 1, \quad (6.17)$$

which follows immediately by (6.2). Second, we make use of the disjoint partition of Γ_i and noting that

$$|U_\delta(\Gamma_{ij})| \lesssim h_i \max(h_i^{d-1}, |\Gamma_i|), \quad (6.18)$$

we obtain

$$\sum_{i=1}^N \sum_{j=0}^{i-1} h_i^{2(m-1)} |\eta_i|_{H^m(U_\delta(\Gamma_{ij}))}^2 \quad (6.19)$$

$$\lesssim \sum_{i=1}^N \sum_{j=0}^{i-1} h_i^{2k} |v_i|_{H^{k+1}(U_\delta(\Gamma_{ij}))}^2 \quad (6.20)$$

$$\lesssim \sum_{i=1}^N \sum_{j=0}^{i-1} h_i^{2k} h_i \max(h_i^{d-1}, |\Gamma_{ij}|) |v_i|_{W_\infty^{k+1}(U_\delta(\Gamma_{ij}))}^2 \quad (6.21)$$

$$\lesssim \sum_{i=1}^N \left(h_i \sum_{j=0}^{i-1} \max(h_i^{d-1}, |\Gamma_{ij}|) \right) h_i^{2k} |v_i|_{W_\infty^{k+1}(U_\delta(\Gamma_i))}^2 \quad (6.22)$$

$$\lesssim \sum_{i=1}^N (h_i^d N_{\mathcal{O}_i} + h_i |\Gamma_i|) h_i^{2k} |v_i|_{W_\infty^{k+1}(U_\delta(\Gamma_i))}^2. \quad (6.23)$$

Due to the maximum norm, this estimate also holds with η_i replaced by η_j , and the desired estimate holds. \square

Remark 6.2. *In practical situations, it is not unreasonable to assume the additional regularity $W_\infty^{k+1}(U_h(\Gamma))$.*

7. *A priori* error estimates

We may now prove the following optimal order *a priori* error estimates. The estimates are supported by the numerical results presented in Figure 8. For details on these results, we refer to the accompanying paper [30].

Theorem 7.1 (*A priori* error estimates). *The finite element solution u_h of (3.2) satisfies the following a priori error estimates:*

$$\| \|u - u_h\| \|_h^2 \lesssim C_{h,N} \sum_{i=0}^N h_i^{2k} |u|_{H^{k+1}(\Omega_{h,i}) \cap W_\infty^{k+1}(U_h(\Gamma_i))}^2, \quad (7.1)$$

$$\| \|u - u_h\| \|_\Omega^2 \lesssim (N_{\mathcal{O}} + 1)^{1/2} C_{h,N} h \sum_{i=0}^N h_i^{2k} |u|_{H^{k+1}(\Omega_{h,i}) \cap W_\infty^{k+1}(U_h(\Gamma_i))}^2. \quad (7.2)$$

Proof. The proof of (7.1) follows the standard procedure of splitting the error and using the energy norm interpolation error estimate from Proposition 6.1,

$$\| \|u - u_h\| \|_h \leq \| \|u - \pi_h u\| \|_h + \| \|\pi_h u - u_h\| \|_h. \quad (7.3)$$

To estimate the second term on the right-hand side of (7.3), we use the coercivity (Proposition 5.4), Galerkin orthogonality (Proposition 4.2) and continuity (Proposition 4.3) of A_h to obtain

$$\| \|\pi_h u - u_h\| \|_h^2 \lesssim A_h(\pi_h u - u_h, \pi_h u - u_h) \quad (7.4)$$

$$= A_h(\pi_h u - u, \pi_h u - u_h) \quad (7.5)$$

$$\lesssim \| \|\pi_h u - u\| \|_h \| \|\pi_h u - u_h\| \|_h. \quad (7.6)$$

It follows that

$$\| \|\pi_h u - u_h\| \|_h \lesssim \| \|u - \pi_h u\| \|_h. \quad (7.7)$$

Combining (7.3) and (7.7) with the interpolation error estimate of Proposition 6.1 now yields (7.1).

To prove (7.2), we use a standard duality argument (see e.g. [9]). Let $\phi \in V = H^{3/2+\epsilon}(\Omega) \cap V_h$ be the solution to the dual problem

$$A_h(v, \phi) = (v, \psi)_\Omega \quad \forall v \in V. \quad (7.8)$$

We now take $v = e = u - u_h$ and use the Galerkin orthogonality (Proposition 4.2), continuity (Proposition 4.3) and a standard interpolation inequality on each set $\Omega_{h,i}$ (note that we cannot use stronger regularity than $\phi \in H^2(\Omega)$ since $\psi \in L^2(\Omega)$ and thus the interpolation bound (6.1) is not applicable for ϕ)

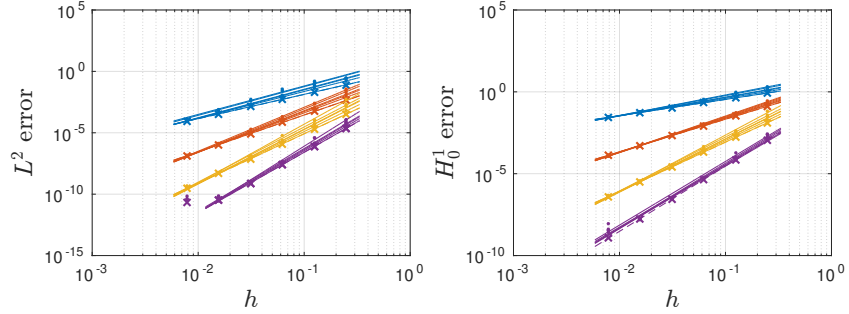


Figure 8: Rate of convergence in the $L^2(\Omega)$ (left) and $H_0^1(\Omega)$ (right) norms for $p = 1$ (blue), $p = 2$ (red), $p = 3$ (yellow) and $p = 4$ (purple). For each p , the convergence rate is shown for $N = 1, 2, 4, 6, 16, 32$ meshes (six lines) and the errors for $N = 0$ (the standard single mesh discretization) are marked with \times and dashed lines.

to obtain

$$(e, \psi)_\Omega = A_h(e, \phi) \quad (7.9)$$

$$= A_h(e, \phi - \pi_h \phi) \quad (7.10)$$

$$\leq \|e\|_h \|\phi - \pi_h \phi\|_h \quad (7.11)$$

$$\lesssim \|e\|_h \left(\sum_{i=0}^N h_i^2 |\phi|_{H^2(\Omega_{h,i})}^2 \right)^{1/2} \quad (7.12)$$

$$\lesssim \|e\|_h \left(\sum_{i=0}^N h_i^2 |\phi|_{H^2(\Omega_{h,i} \setminus \Omega_i)}^2 + \sum_{i=0}^N h_i^2 |\phi|_{H^2(\Omega_i)}^2 \right)^{1/2} \quad (7.13)$$

$$\lesssim \|e\|_h \left((N_{\mathcal{O}} + 1) h^2 |\phi|_{H^2(\Omega)}^2 \right)^{1/2} \quad (7.14)$$

$$\lesssim \|e\|_h (N_{\mathcal{O}} + 1)^{1/2} h \|\psi\|_\Omega, \quad (7.15)$$

where we used the fact that the maximum number of overlapping meshes is $N_{\mathcal{O}}$ and in the last step we have used the standard elliptic regularity estimate (see e.g. [9]). Note that we have continuity (7.11) also for functions in $H^{3/2+\epsilon}(\Omega)$, $\epsilon > 0$, as noted in Proposition 4.3. The desired estimate (7.2) now follows from (7.15) by (7.1) and taking $\psi = e$. \square

8. Condition number estimate

To prove a bound on the condition number, we first introduce some notation and definitions. Let $\{\varphi_{i,j}\}_{j=1}^{M_i}$ be the finite element basis of $V_{h,i}$. We then have

the expansion

$$v_i = \sum_{j=1}^{M_i} \widehat{v}_{i,j} \varphi_{i,j}, \quad (8.1)$$

for each part v_i of a multimesh function $v = (v_0, \dots, v_N)$. Collecting all expansion coefficients for the $1 + N$ parts into a vector \widehat{v} of dimension $M = \sum_{i=0}^N M_i$, the total stiffness matrix \widehat{A} for the multimesh system is defined by

$$(\widehat{A}\widehat{v}, \widehat{w})_M = A_h(v, w) \quad \forall v, w \in V_h, \quad (8.2)$$

with condition number

$$\kappa(\widehat{A}) = |\widehat{A}|_M |\widehat{A}^{-1}|_M. \quad (8.3)$$

To derive an estimate of $\kappa(\widehat{A})$ we make use of the following Lemmas.

Lemma 8.1 (Inverse inequality). *It holds that*

$$\|v\|_h^2 \lesssim (1 + N_{\mathcal{O}}) \max_{0 \leq i \leq N} h_i^{-2} \|v\|_h^2 \quad \forall v \in V_h. \quad (8.4)$$

Proof. Recall the definition of the energy norm (4.1). We first note that

$$I = \sum_{i=0}^N \|\nabla v_i\|_{\Omega_i}^2 \leq \sum_{i=0}^N \|\nabla v_i\|_{\Omega_{h,i}}^2. \quad (8.5)$$

For term *II*, we have by recalling (6.11)

$$II \lesssim \sum_{i=0}^{N-1} \|\nabla v_i\|_{\Omega_{h,i}}^2 + \sum_{i=0}^{N-1} \sum_{j=i+1}^N \delta_{ij} \|\nabla v_j\|_{U_\delta(\Gamma_{ij}) \cap \Omega_j}^2. \quad (8.6)$$

$$\lesssim N_{\mathcal{O}} \sum_{i=0}^N \|\nabla v_i\|_{\Omega_{h,i}}^2. \quad (8.7)$$

Term *III* may be estimated similarly to obtain

$$III \lesssim N_{\mathcal{O}} \sum_{i=1}^N \|\nabla v_i\|_{\Omega_{h,i}}^2. \quad (8.8)$$

For term *IV*, we have by recalling (6.15)

$$IV \lesssim N_{\mathcal{O}} \sum_{i=1}^N h_i^{-2} \|v_i\|_{\Omega_{h,i}}^2 + \sum_{i=1}^N \sum_{j=0}^{i-1} \delta_{ji} h_j^{-2} \|v_j\|_{U_\delta(\Gamma_{ij})}^2 \quad (8.9)$$

$$\lesssim N_{\mathcal{O}} \sum_{i=0}^N h_i^{-2} \|v_i\|_{\Omega_{h,i}}^2. \quad (8.10)$$

The desired estimate now follows using the standard inverse inequality (5.10). \square

Lemma 8.2 (Poincaré inequality). *It holds that*

$$\|v\|_h^2 \lesssim C_P \|v\|_h^2 \quad \forall v \in V_h. \quad (8.11)$$

where

$$C_P = 1 + \max_{0 \leq i \leq N} h_i^{2/d} N_{\mathcal{O}_i} + \max_{0 \leq i \leq N} h_i^2 N_{\mathcal{O}_i}. \quad (8.12)$$

Proof. First note that by a Taylor expansion argument and Lemma 5.1, we have

$$\|v\|_h^2 \lesssim \sum_{i=0}^N (\|v_i\|_{\Omega_i}^2 + h_i^2 \|\nabla v_i\|_{\Omega_{h,i}}^2) \quad (8.13)$$

$$\lesssim \sum_{i=0}^N \|v_i\|_{\Omega_i}^2 + N_{\mathcal{O}} \sum_{i=0}^N \left(h_i^2 \|\nabla v_i\|_{\Omega_i}^2 + h_i^2 \sum_{j=i+1}^N \|\nabla(v_i - v_j)\|_{\mathcal{O}_{ij}}^2 \right). \quad (8.14)$$

To control the first term on the right-hand side in (8.14), let $\phi \in H^2(\Omega)$ be the solution to the dual problem

$$-\Delta \phi = \psi \quad \text{in } \Omega, \quad (8.15)$$

$$\phi = 0 \quad \text{on } \partial\Omega, \quad (8.16)$$

where $\psi \in L^2(\Omega)$. Multiplying the dual problem with $v \in V_h$ and integrating by parts, we obtain using the Cauchy-Schwarz inequality

$$\sum_{i=0}^N (v_i, \psi)_{\Omega_i} = \sum_{i=0}^N (v_i, -\Delta \phi)_{\Omega_i} \quad (8.17)$$

$$= \sum_{i=0}^N (\nabla v_i, \nabla \phi)_{\Omega_i} - \sum_{i=1}^N \sum_{j=0}^{i-1} ([v], n_i \cdot \nabla \phi)_{\Gamma_{ij}} \quad (8.18)$$

$$\leq \sum_{i=0}^N \|\nabla v_i\|_{\Omega_i} \|\nabla \phi\|_{\Omega_i} + \sum_{i=1}^N \sum_{j=0}^{i-1} (h_i + h_j)^{-1/2} \|[v]\|_{\Gamma_{ij}} (h_i + h_j)^{1/2} \|\nabla \phi\|_{\Gamma_{ij}} \quad (8.19)$$

$$\lesssim \left(\sum_{i=0}^N \|\nabla v_i\|_{\Omega_i}^2 + \sum_{i=1}^N \sum_{j=0}^{i-1} (h_i + h_j)^{-1} \|[v]\|_{\Gamma_{ij}}^2 \right)^{1/2} \\ \times \left(\|\nabla \phi\|_{\Omega}^2 + \sum_{i=1}^N \sum_{j=0}^{i-1} (h_i + h_j) \|\nabla \phi\|_{\Gamma_{ij}}^2 \right)^{1/2}. \quad (8.20)$$

Now we continue with the second factor in (8.20). Using the trace inequality

$$\|v\|_{\gamma \cap K}^2 \lesssim h^{-1} \|v\|_K^2 + h \|\nabla v\|_K^2, \quad (8.21)$$

with constant independent of the position of an interface γ (see [27]), we have

$$\sum_{i=1}^N \sum_{j=0}^{i-1} h_l \|\nabla \phi\|_{\Gamma_{ij}}^2 \lesssim \sum_{i=1}^N \sum_{j=0}^{i-1} \delta_{ji} (\|\nabla \phi\|_{\mathcal{K}_{h,i}(\Gamma_{ij})}^2 + h_l^2 \|\nabla^2 \phi\|_{\mathcal{K}_{h,i}(\Gamma_{ij})}^2) \quad l = i, j. \quad (8.22)$$

By the construction of $U_\delta(\Gamma_{ij})$, see (6.4), we have $\mathcal{K}_{h,i}(\Gamma_{ij}) \subseteq U_\delta(\Gamma_{ij})$ with $\delta \sim h_i$. Furthermore, by the Hölder inequality [10] with coefficients r, s such that $1/r + 1/s = 1$ we have

$$\|\nabla \phi\|_{\mathcal{K}_{h,i}(\Gamma_{ij})}^2 \lesssim \|\nabla \phi\|_{U_\delta(\Gamma_{ij})}^2 \quad (8.23)$$

$$= \|1 \cdot |\nabla \phi|^2\|_{L^1(U_\delta(\Gamma_{ij}))} \quad (8.24)$$

$$\leq \|1\|_{L^s(U_\delta(\Gamma_{ij}))} \|\nabla \phi\|_{L^r(U_\delta(\Gamma_{ij}))}^2 \quad (8.25)$$

$$= |U_\delta(\Gamma_{ij})|^{1/s} \|\nabla \phi\|_{L^r(U_\delta(\Gamma_{ij}))}^2 \quad (8.26)$$

$$\lesssim h_i^{1/s} |\Gamma_{ij}|^{1/s} \|\nabla \phi\|_{L^r(U_\delta(\Gamma_{ij}))}^2 \quad (8.27)$$

$$\lesssim h_i^{1-2/p} \|\nabla \phi\|_{L^p(U_\delta(\Gamma_{ij}))}^2 \quad (8.28)$$

$$\lesssim h_i^{1-2/p} \|\phi\|_{W_p^1(U_\delta(\Gamma_{ij}))}^2 \quad (8.29)$$

with $p = 2r$ and $1/s = 1 - 1/r = 1 - 2/p$.

To determine p in (8.29), we use the Sobolev embedding $W_q^l(\Omega) \subseteq W_p^k(\Omega)$ [10] with $k = 1$, $l = 2$ and $q = 2$. This is motivated by the fact that due to elliptic regularity and $\psi \in L^2(\Omega)$, we have $\phi \in H^2(\Omega)$. Since the embedding holds for $1/p - k/d = 1/q - l/d$ [10], we obtain $p = 2d/(d-2)$, where $p = \infty$ for $d = 2$. Thus

$$h_i^{1-2/p} \|\phi\|_{W_p^1(U_\delta(\Gamma_{ij}))}^2 \lesssim h_i^{2/d} \|\phi\|_{W_{2d/(d-2)}^2(U_\delta(\Gamma_{ij}))}^2 \quad (8.30)$$

$$\lesssim h_i^{2/d} \|\phi\|_{H^2(U_\delta(\Gamma_{ij}))}^2. \quad (8.31)$$

Cf. [10] regarding the last inequality for $d = 2, 3$. Returning to the second factor in (8.20) we thus have, using (8.22), (8.29) and (8.31) together with a standard duality argument (see e.g. [9]), elliptic regularity, a stability estimate,

the Poincaré equality and ignoring higher order terms that

$$\|\nabla\phi\|_{\Omega}^2 + \sum_{i=1}^N \sum_{j=0}^{i-1} (h_i + h_j) \|\nabla\phi\|_{\Gamma_{ij}}^2 \quad (8.32)$$

$$\lesssim \|\nabla\phi\|_{\Omega}^2 + \sum_{i=1}^N \sum_{j=0}^{i-1} \delta_{ji} \left(h_i^{2/d} \|\phi\|_{H^2(U_{\delta}(\Gamma_{ij}))}^2 + (h_i^2 + h_j^2) \|\nabla^2\phi\|_{\mathcal{K}_{h,i}(\Gamma_{ij})}^2 \right) \quad (8.33)$$

$$\lesssim \|\psi\|_{\Omega}^2 + \sum_{i=1}^N \sum_{j=0}^{i-1} \delta_{ji} \left(h_i^{2/d} \|\psi\|_{U_{\delta}(\Gamma_{ij})}^2 + (h_i^2 + h_j^2) \|\psi\|_{\mathcal{K}_{h,i}(\Gamma_{ij})}^2 \right) \quad (8.34)$$

$$\lesssim \|\psi\|_{\Omega}^2 + \sum_{i=1}^N \left(N_{\mathcal{O}_i} h_i^{2/d} \|\psi\|_{\Omega_i}^2 + N_{\mathcal{O}_i} h_i^2 \|\psi\|_{\Omega_i}^2 \right) \quad (8.35)$$

$$\lesssim \sum_{i=0}^N (1 + h_i^{2/d} N_{\mathcal{O}_i} + h_i^2 N_{\mathcal{O}_i}) \|\psi\|_{\Omega_i}^2 \quad (8.36)$$

$$\lesssim C_P \|\psi\|_{\Omega}^2. \quad (8.37)$$

The bound on $\sum_i (v_i, \psi)_{\Omega_i}$ in the left-hand side in (8.17) with $\psi = v$ now reads

$$\sum_{i=0}^N \|v_i\|_{\Omega_i}^2 \lesssim C_P \left(\sum_{i=0}^N \|\nabla v_i\|_{\Omega_i}^2 + \sum_{i=1}^N \sum_{j=0}^{i-1} (h_i + h_j)^{-1} \|[v]\|_{\Gamma_{ij}}^2 \right)^{1/2} \quad (8.38)$$

since $\|v\|_{\Omega}$ is bounded.

To conclude, recall (8.14) and insert (8.38) to obtain the desired estimate

$$\|v\|_h^2 \lesssim C_P \left(\sum_{i=0}^N \|\nabla v_i\|_{\Omega_i}^2 + \sum_{i=1}^N \sum_{j=0}^{i-1} (h_i + h_j)^{-1} \|[v]\|_{\Gamma_{ij}}^2 \right) \quad (8.39)$$

$$\begin{aligned} &+ N_{\mathcal{O}} \sum_{i=0}^N \left(h_i^2 \|\nabla v_i\|_{\Omega_i}^2 + h_i^2 \sum_{j=i+1}^N \|\nabla(v_i - v_j)\|_{\mathcal{O}_{ij}}^2 \right) \\ &\lesssim C_P \|v\|_h^2. \end{aligned} \quad (8.40)$$

□

Theorem 8.3 (Condition number estimate). *It holds that*

$$\kappa(\widehat{A}) \lesssim C_P (1 + N_{\mathcal{O}})^2 h^{-2}. \quad (8.41)$$

Proof. Since $\mathcal{K}_{h,i}$ is conforming and quasi-uniform we have the equivalence

$$\|v_i\|_{\Omega_{h,i}}^2 \sim h_i^d |\widehat{v}_i|_{M_i}^2 \quad \forall v_i \in V_{h,i}; \quad (8.42)$$

see e.g. [9]). It follows that

$$\|v\|_h^2 = \sum_{i=0}^N \|v_i\|_{\Omega_{h,i}}^2 \sim \sum_{i=0}^N h_i^d |\widehat{v}_i|_{M_i}^2 \sim h^d |\widehat{v}|_M^2. \quad (8.43)$$

Recall the definition of the matrix norm

$$|\widehat{A}|_M = \sup_{\widehat{v} \neq 0} \frac{|\widehat{A}\widehat{v}|_M}{|\widehat{v}|_M}. \quad (8.44)$$

To estimate $|\widehat{A}|_M$, we use the definition of the stiffness matrix (8.2), the inverse inequality (8.4) and the equivalence (8.43) to obtain

$$|\widehat{A}\widehat{v}|_M = \sup_{\widehat{w} \neq 0} \frac{(\widehat{A}\widehat{v}, \widehat{w})_M}{|\widehat{w}|_M} \quad (8.45)$$

$$= \sup_{\widehat{w} \neq 0} \frac{A_h(v, w)}{|\widehat{w}|_M} \quad (8.46)$$

$$\lesssim \sup_{\widehat{w} \neq 0} \frac{\|v\|_h \|w\|_h}{|\widehat{w}|_M} \quad (8.47)$$

$$\lesssim \sup_{\widehat{w} \neq 0} \frac{(1 + N_{\mathcal{O}})h^{-2} \|v\|_h \|w\|_h}{|\widehat{w}|_M} \quad (8.48)$$

$$\lesssim (1 + N_{\mathcal{O}})h^{d-2} |\widehat{v}|_M. \quad (8.49)$$

Dividing by $|\widehat{v}|$ and using the definition of the matrix norm (8.44) yields

$$|\widehat{A}|_M \lesssim (1 + N_{\mathcal{O}})h^{d-2}. \quad (8.50)$$

To estimate $|\widehat{A}^{-1}|_M$, we proceed similarly, and additionally use the Poincaré inequality Lemma 8.2 and the coercivity of the bilinear form (5.12) to obtain

$$h^d |\widehat{v}|_M^2 \sim \|v\|_h^2 \quad (8.51)$$

$$\lesssim C_P \|v\|_h^2 \quad (8.52)$$

$$\lesssim C_P A_h(v, v) \quad (8.53)$$

$$= C_P (\widehat{A}\widehat{v}, \widehat{v})_M \quad (8.54)$$

$$\leq C_P |\widehat{A}\widehat{v}|_M |\widehat{v}|_M. \quad (8.55)$$

The inequality thus reads

$$h^d |\widehat{v}|_M \lesssim C_P |\widehat{A}\widehat{v}|_M. \quad (8.56)$$

Setting $\widehat{v} = \widehat{A}^{-1}\widehat{w}$ yields

$$h^d |\widehat{A}^{-1}\widehat{w}|_M \lesssim C_P |\widehat{w}|_M. \quad (8.57)$$

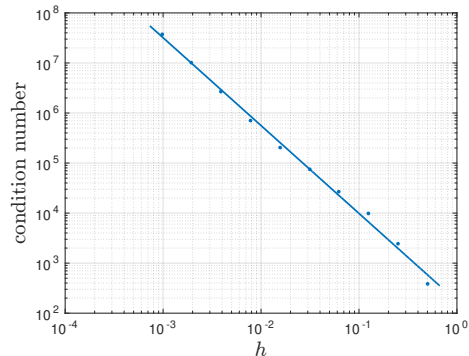


Figure 9: Condition number as a function of the mesh size h [30].

Dividing by $|\widehat{w}|_M$ and using the definition of the matrix norm (8.44) now gives

$$|\widehat{A}^{-1}|_M \lesssim C_P(1 + N_{\mathcal{O}})h^{-d}. \quad (8.58)$$

By using (8.50) and (8.58) in the definition of the condition number (8.3), we obtain the desired estimate (8.41). \square

The estimate for the condition number is supported by the numerical results presented in Figure 9. The slope is found to be -1.76 . The details on this example is found in [30].

9. Numerical results

To demonstrate the applicability and robustness of the multimesh finite element formulation, we present here a couple of numerical examples. For additional examples, we refer to the companion paper [30].

9.1. Convergence under variable mesh size

For the first example, we construct two multimesh configurations I and II , each consisting of three parts (overlapping meshes) as show in Figure 10. We consider a simple Poisson problem with analytical solution

$$u(x, y) = \sin(\pi x) \sin(\pi y). \quad (9.1)$$

The goal is to study the convergence under refinement of the three meshes for each of the two test cases. Starting from initial coarse meshes with equal mesh sizes, we refine each part separately, using 8 different mesh sizes, and compute

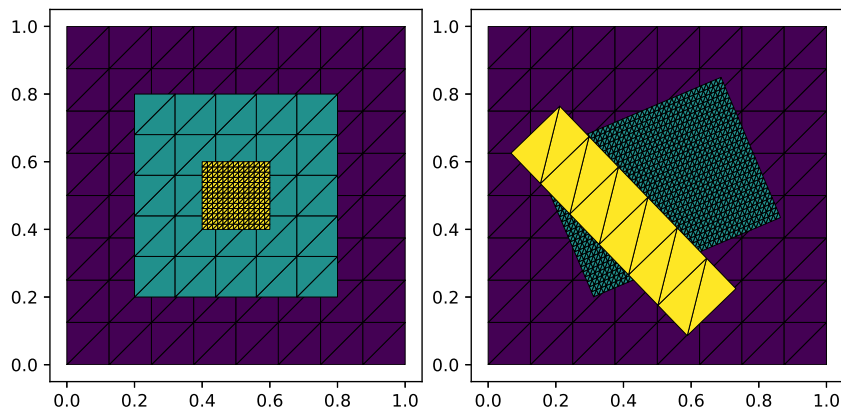


Figure 10: Configuration I (left) and configuration II (right) exemplified by refined part 2 for I and refined part 1 for II . The coarse and fine meshes have mesh sizes 2^{-3} and 2^{-6} respectively.

the $L^2(\Omega)$ and $H_0^1(\Omega)$ error norms. A piecewise linear finite element basis is used for both configurations.

The refinement procedure is as follows. First we will refine part 0 in 8 steps, then part 1 in 8 steps, and finally part 2 in 8 steps. Then we swap the order and refine part 1 first, followed by parts 0 and 2. We do this for all permutations of the order of the parts; in total there are $3!$ combinations. This procedure is performed for both I and II .

Configuration I is a nested configuration (but not hierarchical). Configuration II is generated by placing the second and third parts in a “random” position on top of the background mesh of $\Omega_0 = [0, 1]^2$. Specifically, we have

$$\Omega_1^I = [0.2, 0.8]^2, \quad (9.2)$$

$$\Omega_2^I = [0.4, 0.6]^2, \quad (9.3)$$

$$\Omega_1^{II} = [0.2, 0.8] \times [0.3, 0.75], \text{ rotated } 23^\circ, \quad (9.4)$$

$$\Omega_2^{II} = [0.3, 0.5] \times [0.05, 0.8], \text{ rotated } 44^\circ, \quad (9.5)$$

as illustrated in Figure 10. The meshes are refined with mesh sizes 2^{-k} , $k = 3, \dots, 10$, i.e., 8 steps. Thus, the mesh size ratio between two parts are in this example at most $2^7 \approx 100$.

In Figure 11 we show the $L^2(\Omega)$ and $H_0^1(\Omega)$ errors for the two configurations. As expected, the different curves start and end in the same point. Moreover, we see that during refinement of the first part, errors decrease but flatten. This is due to the fact that the errors from the other two, unrefined, parts dominate. When the second part starts being refined, the errors drop but will again flatten since the errors are dominated by the third and last unrefined part. Refining

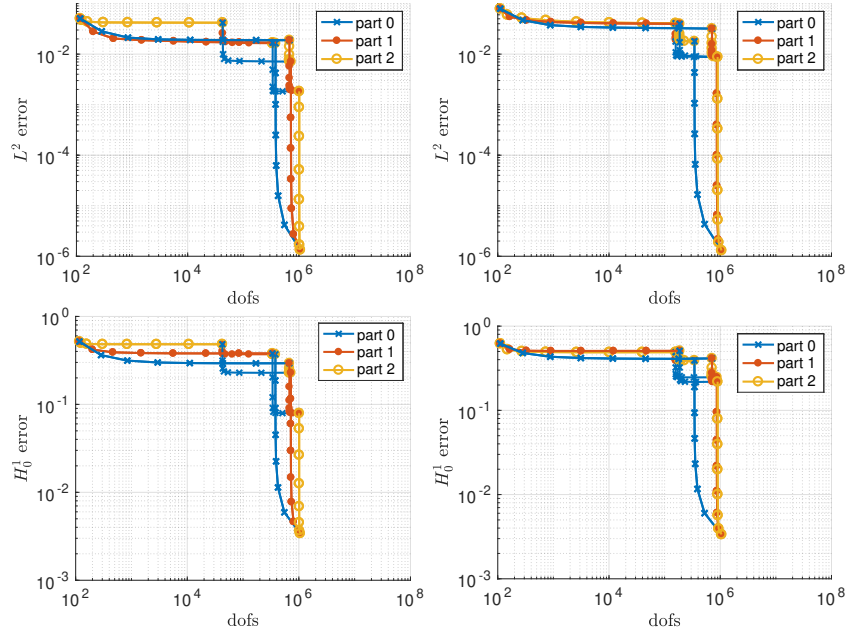


Figure 11: Errors during refinement of multimesh configurations *I* (top row) and *II* (bottom row). Colors and markers indicate which part is being refined. The refinement procedure starts with all parts having a mesh size of 2^{-3} resulting in approximately 10^2 degrees of freedom. Each part is then refined individually and sequentially as described in the text, until all parts have a mesh size of 2^{-10} , resulting in a total of approximately 10^6 degrees of freedom.

this part results in a sharp decrease in the error. Due to the effect of dominating errors from different parts, we observe two L-shaped drops for each refinement permutation, for both configurations and for both error quantities.

There is no significant L-shape decrease for the first refined part, but it would be possible to construct a multimesh configuration such that this would be the case. For the example with this analytical solution, the first part would have a dominating error if the area of the part would be dominating.

It is worth noting is that the errors decrease smoothly and the method is stable despite the large differences in mesh size.

9.2. Boundary layer resolution

To demonstrate the potential of the multimesh formulation for local adaptation, we consider the boundary value problem

$$-\Delta u + \epsilon^{-2}u = f \quad \text{in } \Omega, \quad (9.6a)$$

$$u = 0 \quad \text{on } \Gamma_0, \quad (9.6b)$$

$$u = 1 \quad \text{on } \Gamma_1. \quad (9.6c)$$

For $\epsilon \rightarrow 0$, the PDE reduces to $u = 0$ which is compatible with the boundary condition on Γ_0 . As a consequence, the solution for small ϵ is $u \approx 0$ away from the boundary Γ_1 and then an exponential transition to $u = 1$ close to Γ_1 . The width of the boundary layer is $\sim \epsilon$. The multimesh finite element formulation is identical to (3.2) with the additional term

$$\epsilon^{-2} \sum_{i=0}^N (v_i, w_i)_{\Omega_i}. \quad (9.7)$$

We consider a model problem where the domain Ω is defined by $[0, 1]^2 \setminus \omega$, where ω is the shape of the standard NACA 6409 standard. We let Γ_0 be the boundary of the unit square and let Γ_1 be the boundary of the airfoil. The solution exhibits a boundary layer of width ϵ on the airfoil boundary.

To discretize the problem, we let $\widehat{\mathcal{K}}_{h,0}$ be a uniform mesh of the unit square with mesh size $H = 2^{-(6+k)}$ and let $\widehat{\mathcal{K}}_{h,1}$ be a boundary-fitted mesh of width $w = 0.1 \cdot 2^{-k}$ for $k = 0, 1, 2, 3, 4$. The boundary layer parameter is chosen as $\epsilon = w/2$. The mesh size $h \ll H$ is chosen to well resolve the boundary layer. Note that we intentionally take w small relative to the boundary layer width so as not to get the entire boundary layer transition on the finer mesh, in order to illustrate better the robustness of the method and the coupling of the solution represented on the background mesh and the boundary-fitted mesh on the interface Γ . If instead we take $\epsilon = w/10$, the solution would transition quickly to $u \approx 0$ on the interface Γ .

Figure 12 shows the solution for $k = 1, 2, 3, 4$, clearly demonstrating the decreasing width of the boundary layer with increasing k . Note the smooth transition of the solution going from the representation on the coarse background mesh to the fine boundary-fitted mesh. In Figure 13, a 3D view is plotted for both solution components for $k = 0, 1, 2, 3, 4$. Finally, Figure 14 shows detailed plots of the solution close to the boundary layer for $k = 0$ and $k = 4$.

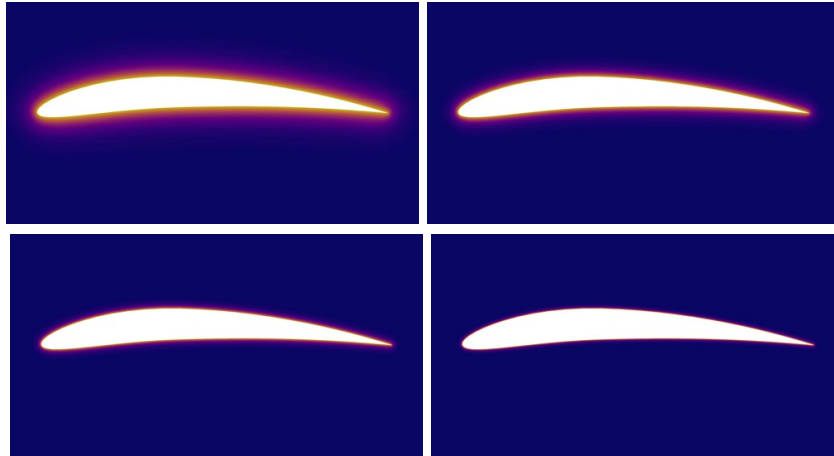


Figure 12: Solution of the boundary layer problem (9.6) for $k = 1, 2, 3, 4$

10. Conclusions and future work

We have analyzed a general framework for discretization of partial differential equations posed on a domain defined by an arbitrary number of intersecting meshes. The framework was analyzed in the context of the Poisson problem. In the accompanying paper [30], numerical results are presented in support of the theoretical analysis presented in the current paper.

11. Acknowledgements

August Johansson was supported by The Research Council of Norway through a Centres of Excellence grant to the Center for Biomedical Computing at Simula Research Laboratory, project number 179578, as well as by the Research Council of Norway through the FRIPRO Program at Simula Research Laboratory, project number 25123. Mats G. Larson was supported in part by the Swedish Foundation for Strategic Research Grant No. AM13-0029, the Swedish Research Council Grants Nos. 2013-4708, 2017-03911, and the Swedish Research Programme Essence. Anders Logg was supported by the Swedish Research Council Grant No. 2014-6093.

References

- [1] D. APPELÖ, J. W. BANKS, W. D. HENSHAW, AND D. W. SCHWENDEMAN, *Numerical methods for solid mechanics on overlapping grids: Linear*

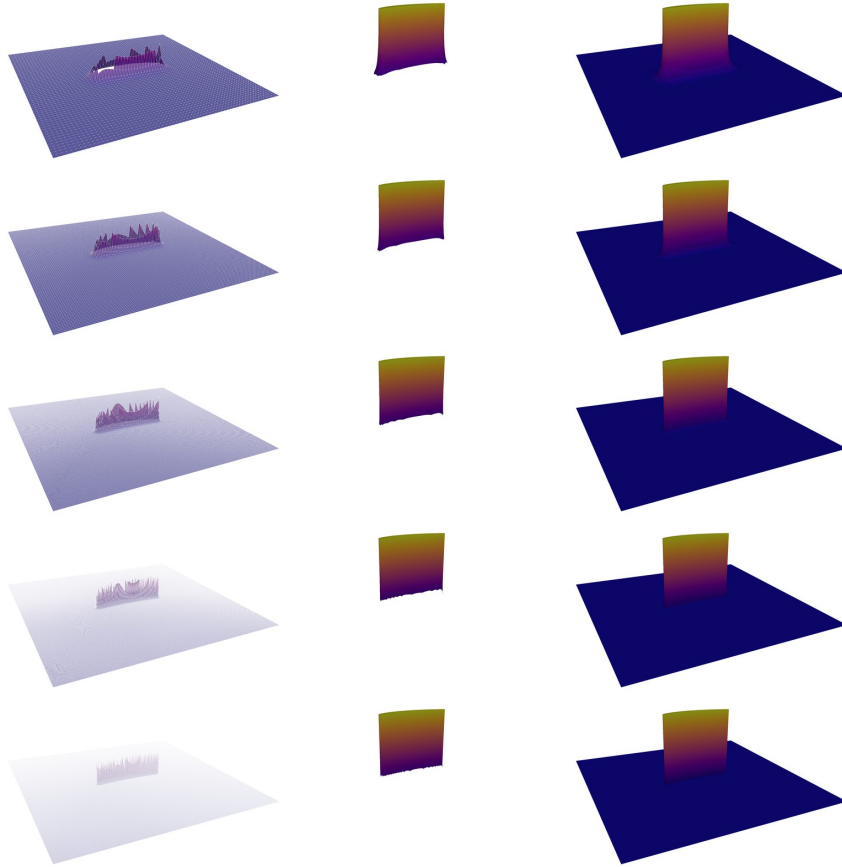


Figure 13: Solution of the boundary layer problem (9.6) for $k = 0, 1, 2, 3, 4$. The left column shows the solution represented on the background mesh, the middle column shows the solution on the overlapping boundary-fitted mesh and the right column shows the composite multimesh solution.

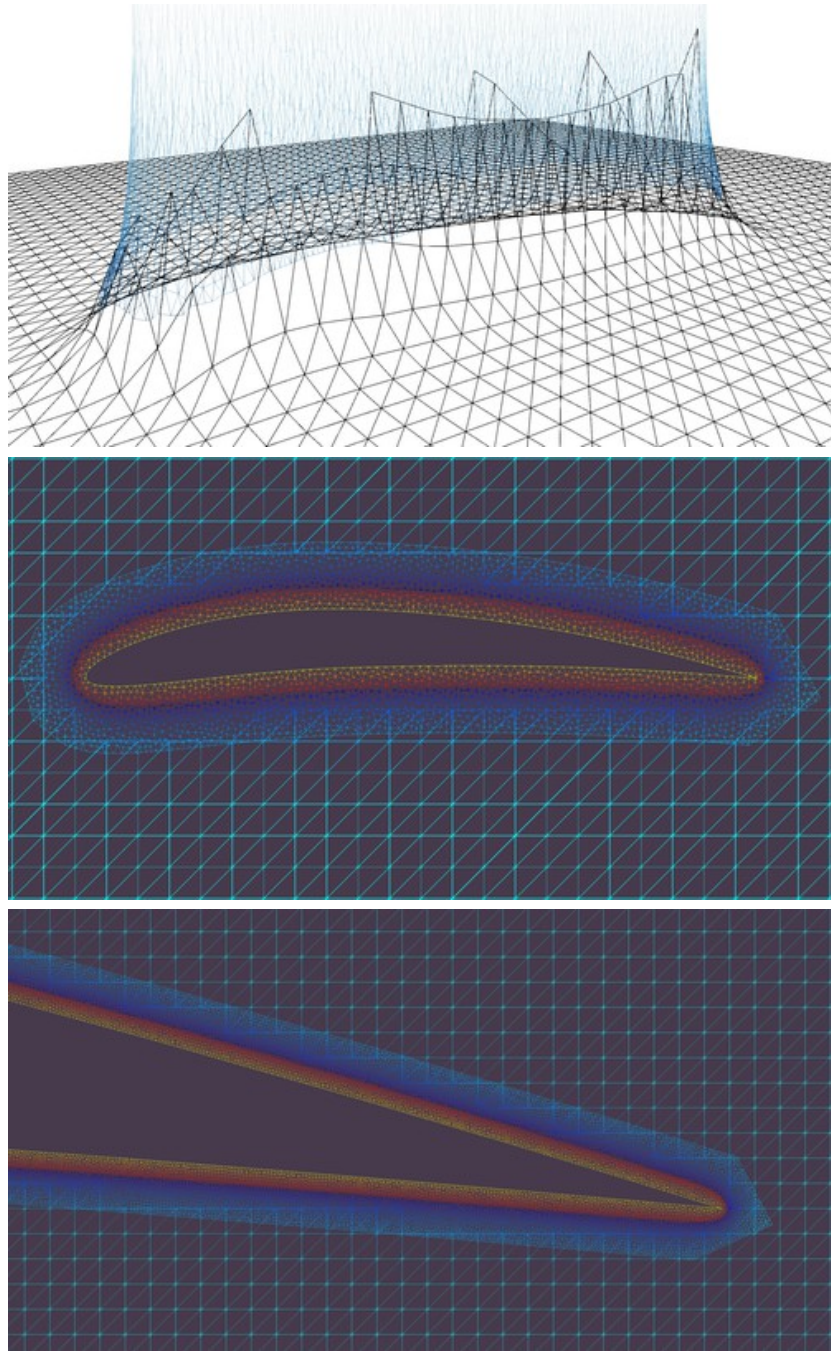


Figure 14: (Top) A 3D view of the matching solutions to the boundary layer problem (9.6) on the background mesh and the overlapping boundary-fitted mesh for $k = 0$. (Middle) The corresponding 2D view for $k = 0$. (Bottom) A detailed zoom close to the tip of the airfoil for the finest mesh ($k = 4$).

- elasticity*, Journal of Computational Physics, 231 (2012), pp. 6012 – 6050, <https://doi.org/10.1016/j.jcp.2012.04.008>.
- [2] D. N. ARNOLD, *An interior penalty finite element method with discontinuous elements*, SIAM J. Numer. Anal., 19 (1982), pp. 742–760, <https://doi.org/10.1137/0719052>.
- [3] P. BASTIAN AND C. ENGWER, *An unfitted finite element method using discontinuous Galerkin*, International Journal for Numerical Methods in Engineering, 79 (2009), pp. 1557–1576, <https://doi.org/10.1002/nme.2631>.
- [4] R. BECKER, E. BURMAN, AND P. HANSBO, *A Nitsche extended finite element method for incompressible elasticity with discontinuous modulus of elasticity*, Comp. Methods Appl. Mech. Engrg., 198 (2009), pp. 3352–3360, <https://doi.org/10.1016/j.cma.2009.06.017>.
- [5] R. BECKER, P. HANSBO, AND R. STENBERG, *A finite element method for domain decomposition with non-matching grids*, ESAIM: M2AN, 37 (2003), pp. 209–225, <https://doi.org/10.1051/m2an:2003023>.
- [6] D. BOFFI, N. CAVALLINI, AND L. GASTALDI, *The finite element immersed boundary method with distributed Lagrange multiplier*, SIAM Journal on Numerical Analysis, 53 (2015), pp. 2584–2604, <https://doi.org/10.1137/140978399>.
- [7] D. BOFFI AND L. GASTALDI, *A finite element approach for the immersed boundary method*, Computers and Structures, 81 (2003), pp. 491–501, [https://doi.org/10.1016/S0045-7949\(02\)00404-2](https://doi.org/10.1016/S0045-7949(02)00404-2).
- [8] S. P. A. BORDAS, E. BURMAN, M. G. LARSON, AND M. A. OLSHANSKII, *Geometrically Unfitted Finite Element Methods and Applications*, vol. 121 of Lecture Notes in Computational Science and Engineering, Springer International Publishing, 2017, <https://doi.org/10.1007/978-3-319-71431-8>.
- [9] S. C. BRENNER AND L. R. SCOTT, *The Mathematical Theory of Finite Element Methods*, Springer, New York, 2008, <https://doi.org/10.1007/978-0-387-75934-0>.
- [10] H. BREZIS, *Functional Analysis, Sobolev Spaces and Partial Differential Equations*, Springer, New York, 2011, <https://doi.org/10.1007/978-0-387-70914-7>.
- [11] E. BURMAN, S. CLAUS, P. HANSBO, M. G. LARSON, AND A. MASSING, *CutFEM: Discretizing geometry and partial differential equations*, International Journal for Numerical Methods in Engineering, 104 (2015), pp. 472–501, <https://doi.org/10.1002/nme.4823>.

- [12] E. BURMAN, J. GUZMN, M. A. SNCHEZ, AND M. SARKIS, *Robust flux error estimation of an unfitted Nitsche method for high-contrast interface problems*, IMA Journal of Numerical Analysis, 38 (2017), pp. 646–668, <https://doi.org/10.1093/imanum/drx017>.
- [13] E. BURMAN AND P. ZUNINO, *Numerical Approximation of Large Contrast Problems with the Unfitted Nitsche Method*, Springer Berlin Heidelberg, Berlin, Heidelberg, 2012, pp. 227–282, https://doi.org/10.1007/978-3-642-23914-4_4.
- [14] J. CHESSA, P. SMOLINSKI, AND T. BELYTSCHKO, *The extended finite element method (xfem) for solidification problems*, International Journal for Numerical Methods in Engineering, 53 (2002), pp. 1959–1977, <https://doi.org/10.1002/nme.386>.
- [15] S. CLAUS AND P. KERFRIDEN, *A stable and optimally convergent latin-cutfem algorithm for multiple unilateral contact problems*, International Journal for Numerical Methods in Engineering, 113 (2018), pp. 938–966, <https://doi.org/10.1002/nme.5694>.
- [16] F. DE PRENTER, C. VERHOOSSEL, E. VAN BRUMMELEN, J. EVANS, C. MESSE, J. BENZAKEN, AND K. MAUTE, *Scalable multigrid methods for immersed finite element methods and immersed isogeometric analysis*, 2019, <https://arxiv.org/abs/arXiv:1903.10977>.
- [17] F. DE PRENTER, C. VERHOOSSEL, G. VAN ZWIETEN, AND E. VAN BRUMMELEN, *Condition number analysis and preconditioning of the finite cell method*, Computer Methods in Applied Mechanics and Engineering, 316 (2017), pp. 297 – 327, <https://doi.org/10.1016/j.cma.2016.07.006>. Special Issue on Isogeometric Analysis: Progress and Challenges.
- [18] J. DOKKEN, S. FUNKE, A. JOHANSSON, AND S. SCHMIDT, *Shape Optimization Using the Finite Element Method on Multiple Meshes with Nitsche Coupling*, SIAM Journal on Scientific Computing, 41 (2019), pp. A1923–A1948, <https://doi.org/10.1137/18M1189208>.
- [19] A. DÜSTER, J. PARVIZIAN, Z. YANG, AND E. RANK, *The finite cell method for three-dimensional problems of solid mechanics*, Computer Methods in Applied Mechanics and Engineering, 197 (2008), pp. 3768 – 3782, <https://doi.org/10.1016/j.cma.2008.02.036>.
- [20] J. FISH, *The s-version of the finite element method*, Computers & Structures, 43 (1992), pp. 539 – 547, [https://doi.org/10.1016/0045-7949\(92\)90287-A](https://doi.org/10.1016/0045-7949(92)90287-A).
- [21] J. FISH, S. MARKOLEFAS, R. GUTTAL, AND P. NAYAK, *On adaptive multilevel superposition of finite element meshes for linear elastostatics*, Applied Numerical Mathematics, 14 (1994), pp. 135 – 164, [https://doi.org/10.1016/0168-9274\(94\)90023-X](https://doi.org/10.1016/0168-9274(94)90023-X).

- [22] L. FORMAGGIA, C. VERGARA, AND S. ZONCA, *Unfitted extended finite elements for composite grids*, Computers and Mathematics with Applications, 76 (2018), pp. 893 – 904, <https://doi.org/https://doi.org/10.1016/j.camwa.2018.05.028>.
- [23] T.-P. FRIES AND T. BELYTSCHKO, *The extended/generalized finite element method: An overview of the method and its applications*, International Journal for Numerical Methods in Engineering, 84 (2010), pp. 253–304, <https://doi.org/10.1002/nme.2914>.
- [24] R. GLOWINSKI, T.-W. PAN, AND J. PERIAUX, *A fictitious domain method for dirichlet problem and applications*, Computer Methods in Applied Mechanics and Engineering, 111 (1994), pp. 283 – 303, [https://doi.org/https://doi.org/10.1016/0045-7825\(94\)90135-X](https://doi.org/https://doi.org/10.1016/0045-7825(94)90135-X).
- [25] C. GRKAN AND A. MASSING, *A stabilized cut discontinuous Galerkin framework for elliptic boundary value and interface problems*, Computer Methods in Applied Mechanics and Engineering, 348 (2019), pp. 466 – 499, <https://doi.org/10.1016/j.cma.2018.12.041>.
- [26] A. HANSBO AND P. HANSBO, *An unfitted finite element method, based on Nitsche’s method, for elliptic interface problems*, Comput. Method. Appl. M., 191 (2002), pp. 5537 – 5552, [https://doi.org/10.1016/S0045-7825\(02\)00524-8](https://doi.org/10.1016/S0045-7825(02)00524-8).
- [27] A. HANSBO, P. HANSBO, AND M. G. LARSON, *A finite element method on composite grids based on Nitsche’s method*, ESAIM-Math. Model. Num., 37 (2003), pp. 495–514, <https://doi.org/10.1051/m2an:2003039>.
- [28] L. HELTAI AND F. COSTANZO, *Variational implementation of immersed finite element methods*, Computer Methods in Applied Mechanics and Engineering, 229-232 (2012), pp. 110 – 127, <https://doi.org/10.1016/j.cma.2012.04.001>.
- [29] W. D. HENSHAW AND D. W. SCHWENDEMAN, *Parallel computation of three-dimensional flows using overlapping grids with adaptive mesh refinement*, J. Comput. Phys., 227 (2008), pp. 7469–7502, <https://doi.org/10.1016/j.jcp.2008.04.033>.
- [30] A. JOHANSSON, B. KEHLET, M. G. LARSON, AND A. LOGG, *Multimesh finite element methods: Solving PDEs on multiple intersecting meshes*, Comp. Methods Appl. Mech. Engrg., 343 (2019), pp. 672 – 689, <https://doi.org/10.1016/j.cma.2018.09.009>.
- [31] A. JOHANSSON AND M. G. LARSON, *A high order discontinuous Galerkin Nitsche method for elliptic problems with fictitious boundary*, Numer. Math., 123 (2013), pp. 607–628, <https://doi.org/10.1007/s00211-012-0497-1>.

- [32] A. JOHANSSON, M. G. LARSON, AND A. LOGG, *High order cut finite element methods for the Stokes problem*, Advanced Modeling and Simulation in Engineering Sciences, 2 (2015), pp. 1–23, <https://doi.org/10.1186/s40323-015-0043-7>.
- [33] C. KADAPA, W. DETTMER, AND D. PERI, *A fictitious domain/distributed Lagrange multiplier based fluidstructure interaction scheme with hierarchical B-Spline grids*, Computer Methods in Applied Mechanics and Engineering, 301 (2016), pp. 1 – 27, <https://doi.org/https://doi.org/10.1016/j.cma.2015.12.023>.
- [34] C. LEHRENFELD, *High order unfitted finite element methods on level set domains using isoparametric mappings*, Computer Methods in Applied Mechanics and Engineering, 300 (2016), pp. 716 – 733, <https://doi.org/10.1016/j.cma.2015.12.005>.
- [35] Z. LI, *The immersed interface method using a finite element formulation*, Applied Numerical Mathematics, 27 (1998), pp. 253 – 267, [https://doi.org/10.1016/S0168-9274\(98\)00015-4](https://doi.org/10.1016/S0168-9274(98)00015-4).
- [36] Z. LI AND K. ITO, *The Immersed Interface Method: Numerical Solutions of PDEs Involving Interfaces and Irregular Domains*, Frontiers in Applied Mathematics, Society for Industrial and Applied Mathematics, 2006, <https://books.google.no/books?id=1kDo-xqgoW8C>.
- [37] W. K. LIU, D. W. KIM, AND S. TANG, *Mathematical foundations of the immersed finite element method*, Computational Mechanics, 39 (2007), pp. 211–222, <https://doi.org/10.1007/s00466-005-0018-5>.
- [38] A. MASSING, M. G. LARSON, A. LOGG, AND M. E. ROGNES, *A stabilized Nitsche overlapping mesh method for the Stokes problem*, Numerische Mathematik, (2014), pp. 1–29, <https://doi.org/10.1007/s00211-013-0603-z>.
- [39] N. MOS, J. DOLBOW, AND T. BELYTSCHKO, *A finite element method for crack growth without remeshing*, International Journal for Numerical Methods in Engineering, 46 (1999), pp. 131–150, [https://doi.org/10.1002/\(SICI\)1097-0207\(19990910\)46:1<131::AID-NME726>3.0.CO;2-J](https://doi.org/10.1002/(SICI)1097-0207(19990910)46:1<131::AID-NME726>3.0.CO;2-J).
- [40] M. NAGAI AND M. KAWAHARA, *A Fictitious Domain Method with Distributed Lagrange Multiplier for Particulate Flow*, International Journal for Computational Methods in Engineering Science and Mechanics, 8 (2007), pp. 115–122, <https://doi.org/10.1080/15502280701246760>.
- [41] J. NITSCHKE, *Über ein Variationsprinzip zur Lösung von Dirichlet-Problemen bei Verwendung von Teilräumen, die keinen Randbedingungen unterworfen sind*, in Abhandlungen aus dem Mathematischen Seminar der Universität Hamburg, vol. 36, Springer, 1971, pp. 9–15, <https://doi.org/10.1007/BF02995904>.

- [42] J. PARVIZIAN, A. DÜSTER, AND E. RANK, *Finite cell method*, Computational Mechanics, 41 (2007), pp. 121–133, <https://doi.org/10.1007/s00466-007-0173-y>.
- [43] C. S. PESKIN, *The immersed boundary method*, Acta Numerica, 11 (2002), p. 479517, <https://doi.org/10.1017/S0962492902000077>.
- [44] E. RANK, *Adaptive remeshing and h-p domain decomposition*, Computer Methods in Applied Mechanics and Engineering, 101 (1992), pp. 299 – 313, [https://doi.org/10.1016/0045-7825\(92\)90027-H](https://doi.org/10.1016/0045-7825(92)90027-H).
- [45] R. SAYE, *Implicit mesh discontinuous Galerkin methods and interfacial gauge methods for high-order accurate interface dynamics, with applications to surface tension dynamics, rigid body fluid-structure interaction, and free surface flow: Part I*, Journal of Computational Physics, 344 (2017), pp. 647 – 682, <https://doi.org/10.1016/j.jcp.2017.04.076>.
- [46] R. SAYE, *Implicit mesh discontinuous Galerkin methods and interfacial gauge methods for high-order accurate interface dynamics, with applications to surface tension dynamics, rigid body fluid-structure interaction, and free surface flow: Part II*, Journal of Computational Physics, 344 (2017), pp. 683 – 723, <https://doi.org/10.1016/j.jcp.2017.05.003>.
- [47] D. SCHILLINGER AND M. RUESS, *The finite cell method: A review in the context of higher-order structural analysis of cad and image-based geometric models*, Archives of Computational Methods in Engineering, 22 (2015), pp. 391–455, <https://doi.org/10.1007/s11831-014-9115-y>.
- [48] F. XU, D. SCHILLINGER, D. KAMENSKY, V. VARDUHN, C. WANG, AND M.-C. HSU, *The tetrahedral finite cell method for fluids: Immersogeometric analysis of turbulent flow around complex geometries*, Computers and Fluids, 141 (2016), pp. 135–154, <https://doi.org/10.1016/j.compfluid.2015.08.027>.
- [49] L. ZHANG, A. GERSTENBERGER, X. WANG, AND W. LIU, *Immersed finite element method*, Computer Methods in Applied Mechanics and Engineering, 193 (2004), pp. 2051–2067, <https://doi.org/10.1016/j.cma.2003.12.044>.